High-pressure densification of silica glass: A molecular-dynamics simulation

Raffaele Guido Della Valle and Elisabetta Venuti
Dipartimento di Chimica Fisica e Inorganica, Università di Bologna, Viale Risorgimento 4, I-40136 Bologna, Italy
(Received 15 January 1996; revised manuscript received 5 April 1996)

We have performed a molecular-dynamics simulation for a sample of amorphous SiO_2 subject to a compression-decompression process at ambient temperature, using a recently proposed two-body potential model. For moderate compression the simulated glass maintains the ideal tetrahedral coordination and displays reversible elastic behavior. For compressions beyond 6 GPa, the glass becomes anelastic and its density and average atomic coordination increase irreversibly. Density, compressibility, and structure of the simulated material compare favorably with the experiments on both undensified and densified SiO_2 glass. The stability of Si-O coordination greater than four in samples subject to high pressure appears to drive the densification process. [S0163-1829(96)06130-9]

I. INTRODUCTION

Amorphous silica (a-SiO_2) has been known for a long time to display anomalous behavior at high pressure.[1] In particular, experiments[2–11] have shown that glass samples compressed beyond $\approx$10–12 GPa and then decompressed exhibit an increase in density by as much as 20%. The original density is not fully recovered even in samples stored at ambient pressure for many years.[8]

The results of various techniques such as neutron and x-ray diffraction,[3–5] Brillouin, Raman, and IR spectroscopy,[6–10] as well as model calculations[4,12–17] suggest that the densification after compression can be attributed to microscopic structural changes and atomic rearrangements, though the mechanism of the process undergone by a-SiO_2 is not yet fully understood.

A clue to such a mechanism is provided by the behavior of crystalline SiO_2 which forms a variety of stable polymorphs with a wide range of densities.[18,19] It is widely accepted[20,21] that silica glass obtained from the melt forms a network of SiO_4 tetrahedra, like in quartz, cristobalite, and coesite, the most common polymorphs of silica. In these low-density structures each Si atom is bound to four O atoms in $Si(O_{1/2})_4$ tetrahedral coordination, while each O atom is bound to two Si atoms which link the tetrahedra in a continuous network. The various SiO_4 polymorphs differ in the relative arrangement of the tetrahedra. Upon compression beyond 16 GPa quartz is irreversibly transformed into stishovite,[22] an extremely dense form of silica which differs from the other polymorphs by containing Si atoms bound to six O atoms in $Si(O_{1/3})_6$ octahedral coordination.

The behavior of the crystalline polymorphs suggests that a possible mechanism for the densification of a-SiO_2 is the formation of some additional Si-O bonds, which leads to the appearance of a small number of Si atoms with coordination greater than four.

Stolper, Ahrens[23] and Jeanloz[24] model geometrically the coordination increase of silicates under pressure, and suggest that the compressed glass, unconstrained by crystal structure, can actually distort more readily into a more compact arrangement. This hypothesis is consistent with the high-pressure x-ray results,[5] which indicate a continuous increase in the Si coordination for pressures greater than 12 GPa. The permanent densification of the glass is explained[23,24] by assuming that part of the high-pressure octahedrally coordinated Si will not spring apart to the tetrahedral configuration when the pressure is released. A mechanism of increase of coordination is also postulated[25] for germania (GeO_2) glass, which is isoelectronic with silica, and which also undergoes an irreversible densification upon compression.

In order to obtain some insight on the densification mechanism, we have performed a molecular-dynamics (MD) simulations[26] of a sample of glassy silica subject to a compression-decompression process.

It is often assumed that the presence of SiO_4 units indicates the dominance of directional covalent bonding over central pairwise-additive interactions, so that three-body potential models should be employed.[27] Models of this type have been proved[15,27–29] to reproduce many properties of silica but, with some exceptions,[27] they are unable to model changes in the Si coordination number, as their analytical form discriminates in favor of SiO_4 tetrahedral coordination.

The reasons for adopting three-body models are not, in our opinion, very compelling. In fact, several calculations[13,16–18,30–45] have shown that two-body interaction potentials are as effective as the three-body ones in describing both crystalline and amorphous silica.

A recent breakthrough is the construction, by Tsuneyuki *et al.*[18] and by van Beest, Kramer, and van Santen,[45] of two-body potential models fitted to *ab initio* calculations on tetrahedral SiO_4^{4-} clusters. The two models have the same analytical form, but different parametrizations. Because of their quantum-mechanical origin, these new two-body models effectively incorporate an average of the many-body interactions.

Most MD and Monte Carlo studies on densified a-SiO_2 have been performed by quenching a high-density, high-temperature melt rather than by compressing a room-temperature glass.[15–17,44] As far as we know, the only available direct simulation of a compression-decompression process at room temperature is an important calculation by Tse, Klug, and Le Page[13] with the potential model of van Beest, Kramer, and van Santen.[45] We have performed a MD calculation similar to that of Tse, Klug, and Le Page,[13] but

more focused on the densification mechanism and on the properties of the densified glass.

Following previous works,[42,43] we have adopted the potential of Tsuneyuki *et al.*[18] The model reproduces structure, density, compressibility, and vibrational frequencies of both the crystalline,[18,40,41] and amorphous[42,43] forms of silica, and has been applied to the study of pressure-induced[39] and thermal-induced[40] phase transitions in crystalline silica. As the potential successfully reproduces the stability for both four-coordinated and six-coordinated crystalline silica at ambient pressure,[18,40] and predicts an increased coordination in compressed liquid,[44] crystalline and amorphous[16,17] silica at high temperatures, we expect it also to be able to describe the densification of amorphous silica without any *a priori* coordination constraint.

In Sec. II the methods and the conditions of the simulation are presented, and in Sec. III we give some details of the treatment undergone by the sample during the simulated compression-decompression cycles. Results and comparisons with the experimental data are presented and discussed in Sec. IV. We conclude in Sec. V by proposing a possible densification mechanism.

II. METHODS

We have simulated a sample of amorphous SiO_2 subject to a compression-decompression process at constant temperature. For this purpose we have performed a MD calculation for 250 Si and 500 O atoms interacting through a pairwise additive atom-atom potential developed by Tsuneyuki *et al.*[18] The initial amorphous sample was a slightly defective continuous random network[46] of corner-sharing SiO_4 tetrahedra, originally obtained by simulating the cooling of liquid silica.[42] The cooling simulation, and the structural and vibrational properties of the simulated glass at room conditions, have been discussed in detail elsewhere.[42,43]

The compression-decompression runs described in this paper have been carried out with the isothermal-isobaric Andersen method,[47] which simulates a sample in contact with an heat bath and subject to an hydrostatic pressure. The bath temperature was maintained at 300 K for all runs, while the applied pressure was either changed continuously with time (for most runs), or suddenly switched to a constant value (''instantaneous'' compression or decompression). The equations of motion were integrated using the velocity Verlet algorithm,[48–50] with a time step of 1 fs. Further details of the simulation procedure appear in Refs. 42 and 43.

III. CALCULATIONS

Starting from the amorphous state obtained by simulated cooling of liquid SiO_2,[42] MD simulation runs were carried out under the following conditions:

(1) equilibration of the initial sample at 300 K and 0 GPa;

(2) instantaneous compression to 25 GPa of the final state of run 1, followed by equilibration;

(3) instantaneous decompression to 0 GPa of the final state of run 2, followed by equilibration;

(4) continuous compression up to 25 GPa of the final state of run 1, with a compression rate of 0.25 GPa/ps, followed by continuous decompression, with the same rate;

(5) continuous compression followed by continuous decompression, similar to run 4, but with a rate of 0.0625 GPa/ps;

(6) decompression to 0 GPa for several states recorded during the continuous compression of runs 4 and 5.

The compression-decompression rates of runs 4 and 5 were chosen after a careful study of the stabilization of density and potential energy during runs 1, 2, and 3, which employed at least 80 000 steps each. We have found that the equilibration of the system is extremely sluggish. This is to be expected, because it is experimentally known[8] that compressed a-SiO_2 is still relaxing after a period of months. Complete equilibration is very difficult to attain even on the long-time scales allowed by laboratory experiments. However, since we only aim to understand the densification mechanism, a precise determination of the predictions of the potential model at each pressure is not necessary. Therefore, rather than wasting computer time in the vain attempt of equilibrating the system at each pressure, we have decided to investigate the relaxation effects by repeating the compression-decompression process with a rate sufficiently slow for partial equilibration (0.25 GPa/ps), and with the slowest rate allowed by our computer time constraints (0.0625 GPa/ps).

IV. RESULTS

The equilibrated glass at room temperature and pressure is similar to the glass obtained in the cooling simulation at constant volume described in Ref. 42, and which was found to reproduce reasonably well the structural and vibrational properties of a-SiO_2.[42,43]

The density calculated at 1 atm ($\approx 10^{-4}$ GPa) with the model of Tsuneyuki *et al.*[18] is 2.35 g/cm^3, a value almost identical to that of 2.36 g/cm^3 obtained by Tse, Klug, and Le Page.[13] These authors note that their value is better than most computed data reported in the literature. The experimental density[51] value at atmospheric pressure is 2.20 g/cm^3, about 7% lower than the calculation results.

A. Density and compressibility results

A convenient summary of the MD results for a-SiO_2 is provided by Fig. 1, where the relative densities at the end of runs 1, 2, and 3 and the running averages during runs 4 and 5 are compared to the available experiments as a function of pressure.[3,4,10] By displaying the densities relative to the value at atmospheric pressure (ρ/ρ_0), rather than the absolute data, we effectively compensate for the initial 7% discrepancy between calculations and experiments. The variations in density among runs with different compression-decompression rates, i.e., 0.25 GPa/ps, 0.0625 GPa/ps and ''instantaneous,'' are very small. Such a small dependence of ρ on the pressure rate indicates that our partially equilibrated system closely resembles a fully equilibrated sample.

The computed densities of Fig. 1 exhibit a characteristic anelastic behavior in the compression-decompression cycle. On compression a partly irreversible densification appears so that, at least on MD time scales, the density of the starting material is never fully recovered upon equilibration after decompression. The residual density increase of the samples

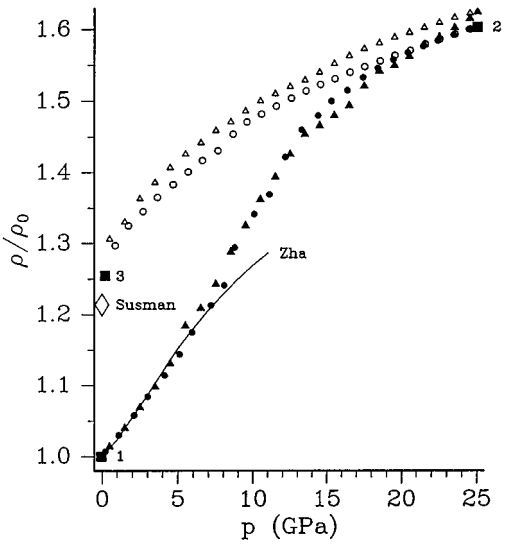

FIG. 1. Relative density ρ/ρ_0 of a-SiO_2 vs pressure p. Squares 1 through 3 indicate equilibrated configurations at the end of runs 1, 2, and 3, i.e., initial equilibration, instantaneous compression and instantaneous decompression. Filled and empty symbols indicate running averages during compression and decompression, respectively, with rates of 0.25 GPa/ps (circles) and 0.0625 GPa/ps (triangles). The line is for static pressure experiments by Zha *et al.* (Ref. 10) under compression. Measurements for decompressed silica are available only for samples recovered at 0 GPa. The diamond is for a sample recovered after room-temperature compression to 16 GPa [Susman and co-workers (Refs. 3 and 4)].

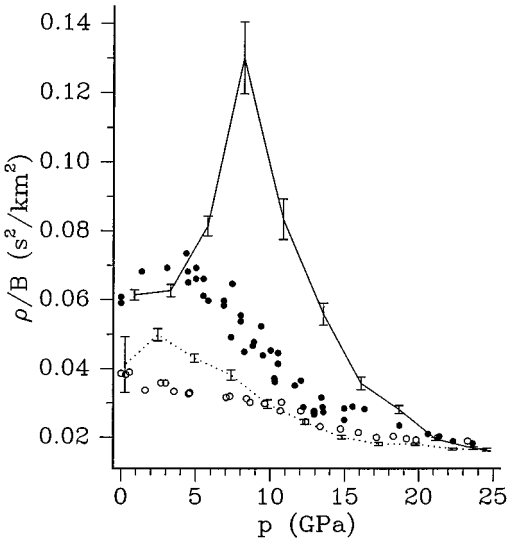

FIG. 2. Ratio ρ/B of density and bulk modulus vs pressure p. Sound velocity measurements (Ref. 52) under increasing and decreasing pressures: filled and empty circles, respectively. Calculated $\rho/B=d\rho/dp$ under increasing and decreasing pressures: solid and dotted lines, respectively. The center and half width of the error bars represent the mean and standard deviation of ρ/B, as obtained from the linear fit to ρ vs p.

decompressed at 0 GPa from a pressure of 25 GPa shows little or no dependence on the compression-decompression rate and is very close to that detected in the experiments at the end of similar pressure cycles (about 20%).[3,4]

Owing to experimental difficulties under nonelastic conditions, separate density and compressibility measurements during decompression are not yet available. Thus the anelastic behavior clearly shown by the MD results for the density cannot yet be followed directly in the experiments. However, a very clear anelasticity is evidenced by sound velocity measurements,[10,52] and in particular by ρ/B, the ratio between density and bulk modulus,[52] which is compared in Fig. 2 with the MD results.

We have computed ρ/B for an isothermal system as $d\rho/dp$, by dividing the compression-decompression run at 0.25 GPa/ps (run 4) in segments of 10 000 steps (i.e., at intervals of 2.5 GPa), and then performing a linear least-squares fit for ρ as a function of p in each segment. This yields two curves which agree with the experimental data at both low and high pressures. At intermediate pressures on the compression side the calculations exhibit the correct trend but do not agree quantitatively with the experiments. As shown by the error bars of Fig. 2, also the uncertainties on ρ/B are larger in this range. This behavior can be attributed to the large density fluctuations accompanying the structural relaxation undergone by the sample during the process, as discussed below in Sec. IV D. As discussed in Ref. 25, the discrepancy between the calculations and the ultrasonic data has to be attributed to the fact that the ultrasonic waves propagate on time scales that are much faster than those required for the structural relaxation. Since the calculations are quasistatic and allow enough time for the occurrence of relaxation, while the ultrasonic measurements reflect an essentially unrelaxed system, the calculated low-frequency bulk modulus B is systematically lower than the high-frequency ultrasonic B in the pressure range where structural relaxation takes place.

The results of Figs. 1 and 2 for ρ and ρ/B vs p suggest that an essentially continuous transformation takes place during the compression-decompression process, in agreement with previous findings[5] and understandings.[23,24] Our results are at odds with those of Tse, Klug, and Le Page,[13] who claim a sudden density increase around 15 GPa. The potential model used here[18] and that used by Tse, Klug, and Le Page[45] look so similar that we are reluctant to attribute such a significant discrepancy to differences in the potentials, even though no other explanation seems very likely.

B. Radial correlation functions

For the normal and densified samples at 0 GPa we have computed the total neutron pair-correlation function $T(r)$, given in Fig. 3 together with the experimental results.[3,4] In our case the densified sample is the one recovered at 0 GPa after applying a pressure of 25 GPa, as described in Sec. III for run 4. The $T(r)$ function has been obtained by first weighting the computed partial pair radial correlation functions $g_{ij}(r)$ with the nuclear-scattering lengths[20] and then by convoluting with the same experimental resolution function that is used in the neutron-scattering experiments.[3,4]

The $R_x=\sqrt{\Sigma_i[T_{\rm obs}(r_i)-T_{\rm calc}(r_i)]^2/\Sigma_i T^2_{\rm obs}(r_i)}$ agreement factor[20,53] between observations[3,4] and calculations is $R_x\approx 15\%$. Since we account for both undensified and densified silica, we consider our result quite satisfactory. The best

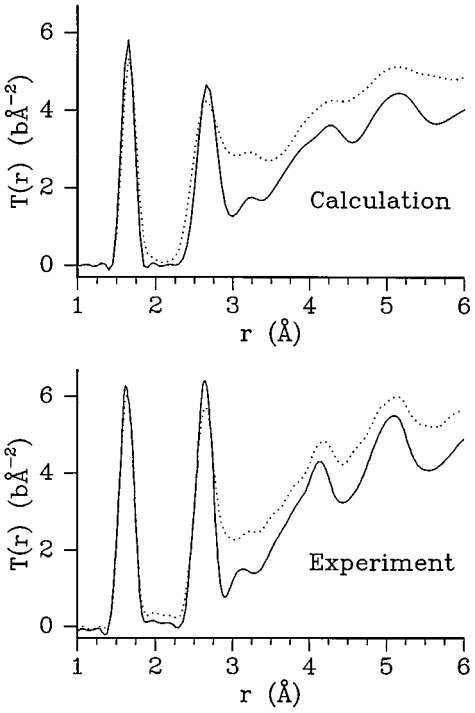

FIG. 3. Total neutron pair radial correlation function $T(r)$ [upper panel: experiment (Refs. 3 and 4), lower panel: calculation] for a-SiO_2 before (solid line) and after (dotted line) the compression-decompression cycle.

MD result to date[20] for undensified silica only is $R_x=9.1\%$ (Ref. 29) (obtained with a three-body potential model). These calculated values should be compared with the typical experimental accuracy, $R_x\approx 1.5\%$.[20]

The experimental $T(r)$ contains information on the distributions of coordination distances and bond angles in the glass. Unfortunately the extraction of this information from the measurements depends on the functional form chosen for the distributions and on the assumed correlation (or lack of correlation) between distances and angles.[20,53–56] At the moment only the experimental peaks around 1.6 and 2.6 Å are clearly assigned[3–5,53] to Si-O and O-O nearest neighbors, respectively, while an unambiguous deconvolution of the measured $T(r)$ has not been possible for densified a-SiO_2 at distances beyond 3 Å.[4] The model dependence of the experimental analysis, which may even lead to differences of several degrees in the average bond angles estimated from the *same* experimental data,[51,56] is probably responsible for the somewhat conflicting results found in the literature.

A cursory glance at Fig. 3 indicates that the calculations agree with the experiments on the global shape of the $T(r)$ and on its overall change upon densification. A more careful analysis reveals that even the changes in the area and width of the peaks are well described. The calculations reproduce well the increased area and the broadening of the O-O peak, which has been attributed to a broadening of the angle distribution,[3] and the increased area at distances between 2.8 and 3.4 Å. The calculations also reproduce the small increase upon densification of the area of the $T(r)$ in the 1.9–2.3 Å range observed by Susman *et al.*[4] and which was tentatively assigned to a small number of additional Si-O bonds created during the densification process. The success of the calculations in this range is probably due to the absence of coordination constraints in the two-body potential model,[18] since the $T(r)$ area does not increase in the MD simulations with three-body interactions.[4]

C. Structural changes upon densification

The mechanisms which accompany the densification can be identified by comparing the structural properties of the densified glass with those of the starting material. We recall that in the pressure induced transformation from the low-density polymorphs of crystalline silica (quartz, cristobalite and coesite) to the high density form (stishovite) the Si coordination grows from 4 to 6, while the Si-O bond length is forced to increase to accommodate for the additional O neighbors. In the light of the processes which occur for crystalline SiO_2,[18,19,57] we have carefully analyzed the distributions of coordination numbers, of interatomic distances and of bond angles in the simulated samples.

Since the first minimum of the partial pair radial correlation function $g_{SiO}(r)$ is around 2.4 Å, we have chosen to consider closer Si-O pairs as bound neighbors, while O-O (or Si-Si) pairs are taken as neighbors if they are both bound to a common Si (or O) atom.

The structure of the initial sample corresponds to the usual model for SiO_2, consisting of SiO_4 tetrahedra that share corners and are arranged in a random network[46] with very few coordination defects: 99% of the Si atoms have four O atom neighbors, and 99% of the O atoms have two Si neighbors. Virtually no pairs of tetrahedra sharing edges (0.04%) are found. A significant disruption of the tetrahedral order occurs upon densification: in our recovered sample 20% of the Si atoms have five or six O neighbors, while 10% of the O atoms have three Si neighbors. About 4% of all connected pairs of tetrahedra now share edges.

For each pair i-j of atomic species, we have computed the average coordination numbers n_{ij}, and the average and standard deviation of the interatomic distances r_{ij} and of the angles $\widehat{iji}$, both for the starting and recovered a-SiO_2. The calculated distributions, which have been obtained directly from the atomic coordinates during the simulation, are compared in Table I with the results of the analyses of NMR, neutron and x-ray-scattering experiments.[3,4,9,20,51,53,54,56,58] The table shows that the computations are in reasonable agreement with the results of the experimental analyses, for both the starting and the densified material.

In the simulation of the densification process, we find a slight increase of the average Si-O bond length accompanied by a decrease of the average Si-O-Si angle and Si-Si separation. The number of Si-O, O-O, and Si-Si neighbors increases, and the O-Si-O and Si-O-Si angle distributions broaden significantly. These results agree with most, although not all, of the experimental investigations.[3,4,54,55] Experimentally, longer Si-O bonds and reduced Si-O-Si angles are found in electron-spin-resonance measurements on 24% densified glass.[55] The neutron data on 20% densified glass[3,4] suggest a slight increase of the Si-O coordination, accompanied by a lengthening of the Si-O bond and by a decreased O-Si-O angle. X-ray-diffraction experiments on silica glass under pressure in the range 8–28 GPa (Ref. 5) also indicate an increase in the Si-O bond length, which is interpreted as

TABLE I. Average coordination numbers n_{ij}, and average and standard deviation for the bond distances r_{ij} and the bond angles $\widehat{ijl}$ of starting and densified silica glass. Calculations are at 300 K, 0 GPa. Most experiments are for samples compressed at room temperature.

		n_{ij}		r_{ij} (Å)		$\sigma_{r_{ij}}$ (Å)	
i-j		Starting	Densified	Starting	Densified	Starting	Densified
Si-O	Calc.	4.009	4.209	1.648	1.686	0.047	0.104
	Obs.	3.85,[a]3.97[b]	3.93[b]	1.608,[a]1.62[b,c]	1.62,[c]1.63[b]	0.047,[a]0.049[b]	0.053[b]
O-O	Calc.	6.035	6.846	2.682	2.714	0.130	0.265
	Obs.	5.94,[a]6.00[b]	6.59[b]	2.626,[a]2.65[b]	2.64,[c]2.66[b]	0.091,[a]0.087[b]	0.12[b]
Si-Si	Calc.	4.042	4.837	3.145	3.139	0.119	0.173
	Obs.	4.13[d]		3.077,[a]3.07[c]	3.02[c]	0.111[a]	
i-j-i				$\widehat{ijl}$ (degrees)		$\sigma_{\widehat{ijl}}$ (degrees)	
				Starting	Densified	Starting	Densified
O-Si-O	Calc.			109.3	108.3	8.0	16.8
	Obs.			109.7,[a]109.5[b]	109.2[b]	4.5[a]	
Si-O-Si	Calc.			147.8	139.1	14.1	19.8
	Obs.			142,[c]143,[e]144[f]	137,[c]138[e]	26[e]	25[e]

[a]References 20 and 53.
[b]References 3 and 4.
[c]Reference 9.
[d]Reference 58.
[e]Reference 54.
[f]References 51 and 56.

the result of a higher Si coordination.[5] These high-pressure data, although qualitatively different from those on densified glass at ambient pressure, clearly suggest a common mechanism and are consistent with the gradual coordination increase proposed in Refs. 23 and 24.

We have searched for possible links between Si coordination and Si-O bond length in the simulated system and have found a rather direct correlation. By separately analyzing the distributions of Si-O distances around Si atoms with coordination 4 and >4, we have obtained two smooth monomodal distributions centered at different bond lengths. In the undensified glass, the average length is ≈1.65 Å for Si atoms with coordination 4, and ≈1.83 Å for atoms with higher coordination. Because these averages remain essentially identical when going to the densified glass, the direct cause of the increased average and dispersion of the Si-O lengths (Table I) must be the increased population of Si atoms with higher coordination and longer Si-O bonds, rather than an overall lengthening of the bonds.

To obtain more information on the relations between the coordination number and the local glass structure, we have analyzed the O-Si-O bond angle distribution in terms of individual contributions due to Si atoms with four, five, and six O neighbors. As shown in the lower panel of Fig. 4, this analysis indicates that the broadening of the O-Si-O distribution in the densified glass (Table I) is to be attributed to the appearance of Si atoms with coordination of five or higher, rather than to an increased frustration of the tetrahedral packing, which would simply result in a broadening of the distribution of the four-coordinated atoms. The average O-Si-O angle around Si with coordination four remains close to the ideal tetrahedral angle of 109.5°, while the average angle around Si with higher coordination is ≈90°, as expected for an octahedral coordination.

A similar mechanism holds for the Si-O-Si distribution, shown in the upper panel of Fig. 4. Around two-coordinated O we find an asymmetric distribution of O-Si-O angles extending from 120° to 180°, in both undensified and densified glass. In the densified material, due to the abundance of three-coordinated O, which exhibit a broad distribution extending from 80° to 140°, the Si-O-Si distribution broadens and the average angle decreases (Table I). This behavior is consistent with the NMR results.[54]

The angular distributions calculated in this work are roughly similar to that found in the MD simulation of Tse, Klug, and Le Page.[13] A more careful comparison with the previous MD results[13] reveals that the angular distributions calculated for the densified material are quite different, unlike those for undensified glass, which are virtually identical. In particular, Tse, Klug, and Le Page[13] find that the O-Si-O distributions become much more structured upon densification and develop a peak at 165°, which they attribute to the presence of edge sharing tetrahedra. In our sample the occurrence of pairs of edge sharing tetrahedra is found to be significant, as previously mentioned, but no feature due to such pairs is found in the O-Si-O distribution.

D. Onset of anelasticity

To investigate the anelasticity effects, a sequence of configurations was recorded during the continuous compression of runs 4 and 5. These stored states were subject to two

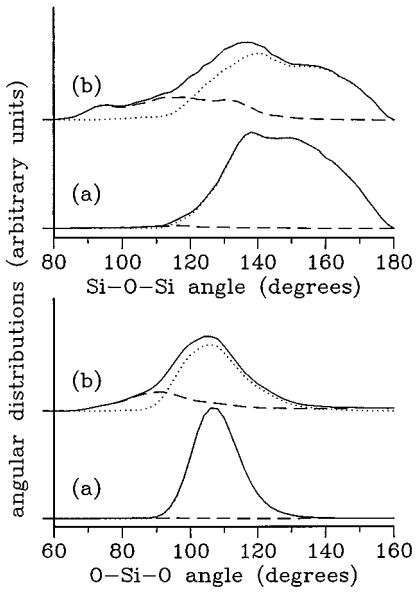

FIG. 4. Average distributions of O-Si-O and Si-O-Si angles for a-SiO_2 before (a) and after (b) the compression-decompression cycle. The total O-Si-O distribution (solid lines) is decomposed in the contributions from Si atoms with coordination 4 (dotted lines), and $\geqslant 5$ (dashed lines). The Si-O-Si distribution (solid lines) is decomposed in the contributions from two- and three-coordinated O atoms (dotted and dashed lines, respectively).

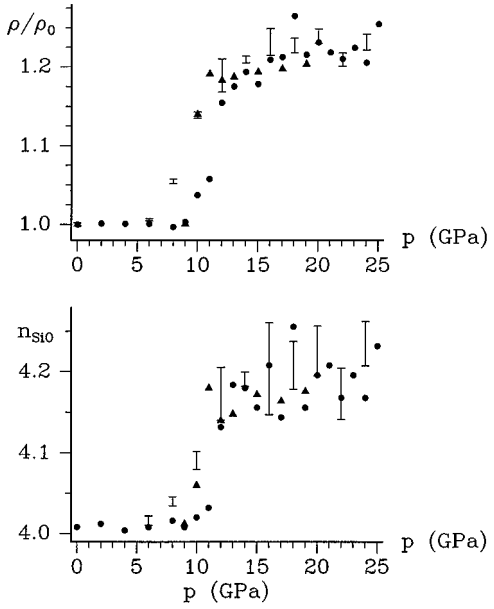

FIG. 5. Equilibrium properties of a-SiO_2 at zero pressure for states recovered after compression. The relative density ρ/ρ_0 (upper panel) and the average number n_{SiO} of O neighbors for Si atoms (lower panel) are shown as a function of the maximum pressure applied. Symbols indicate states recorded during the compression at 0.25 GPa/ps (circles) or 0.0625 GPa/ps (triangles) and subject to instantaneous decompression. The center and half width of the error bars represent means and standard deviations for the samples annealed under pressure and then decompressed.

distinct kinds of processes: (a) instantaneous decompression to 0 GPa and, for some states of run 4, (b) repeated equilibration for 30, 60, 90, and 120 ps at constant volume, followed by instantaneous decompression down to 0 GPa (annealing-decompression process). The system was equilibrated at 0 GPa for 30 ps for both kinds of processes.

The relative densities ρ/ρ_0 calculated for processes (a) and (b) are reported as a function of the pressure applied during the compression run in the upper panel of Fig. 5. In order to analyze the possible correlation between density and Si coordination we show in the lower panel of Fig. 5 the average Si coordination number vs the applied pressure.

The symbols of the upper panel of Fig. 5 originate from the instantaneous decompression process (a). The center and half width of the error bars represent means and standard deviations of the density values for the annealed states (b). Therefore, the bars span the range of density into which the state annealed at high pressure falls when the compression is instantaneously released. The presence of a range of available density values proves that a variety of configurations are accessible to the equilibrating sample.

The plot shows that for compression below 6 GPa the initial equilibrium density is fully recovered, and that above this point irreversible densification occurs. Above 15 GPa the residual density increase is nearly independent of the applied pressure. Experimentally, elastic behavior is observed up to $\approx$8–10 GPa,[7,10,52] and most of the densification takes place between 12 and 24 GPa.[10] The transformation is complete above 30 GPa.[10]

Below 6 GPa and above 14, that is in the p range of elastic behavior and in the one where most irreversible structural changes have already taken place, the trends of the computed densities prove to be virtually independent of the sample history: the density for states instantaneously decompressed to 0 GPa falls into the range defined by the bars. Instead, at intermediate pressures the density of the recovered sample increases with the amount of equilibration to which the state has been subjected. The larger density for the samples equilibrated under pressure and for those subjected to a slower compression rate (run 5) indicates that some annealing takes place during the longer time spent at the high pressures. It is annealing, i.e., the thermally activated process in which the system slowly overcomes the potential energy barriers hindering the structural changes, which is responsible for the large density fluctuations mentioned in Sec. IV A.

Important structural changes induced by compression are evidenced by the plot of the average Si coordination number vs the applied pressure shown in the lower panel of Fig. 5. Again, the error bars represent mean and standard deviation of the coordination number distribution for the states annealed under pressure and then decompressed. The most remarkable feature of the results is the increasing of the average coordination, determined by the appearance of Si atoms with coordination 5 and 6, in the states undergoing irreversible densification. The population of Si atoms with coordination $\geqslant 5$ still present when the pressure is released turns out to be nearly constant above an applied pressures of $\approx$15 GPa.

The data of Fig. 5 clearly show that density and coordination number exhibit a very similar trend with increasing

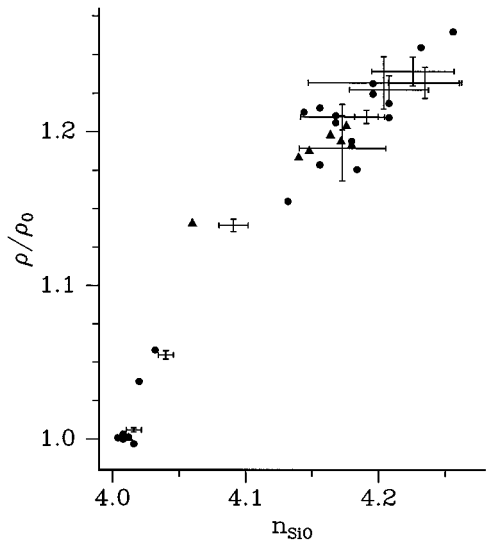

FIG. 6. Correlation between relative density ρ/ρ_0 and average Si-O coordination number n_{SiO} for decompressed a-SiO_2. Symbols and errors bars are as described in Fig. 3.

pressure, thus suggesting a closer analysis of the correlation between these two quantities. This has been done in Fig. 6, where the density of the recovered material is shown to increase monotonically with the Si coordination number. Furthermore, this happens regardless of the history of the sample, as proved by the same behavior displayed both by the symbols and the ''errors bars'' of the figure. This leads to the conclusion that in the simulation the density is predominantly a function of the Si atom coordination.

V. DISCUSSION AND CONCLUSIONS

Our results prove that classical MD calculations with a two-body potential model[18] are capable of describing a densification process irreversible on MD time scales, and which closely emulates the observations on silica glass. Using Tsuneyuki's potential,[18] we have obtained density and compressibility data in reasonable agreement with the experiments, and very good results for radial correlation functions, coordination numbers, bond distances and angles of both undensified and densified glasses.

The MD results appear similar to those obtained by Tse, Klug, and Le Page[13] with the model of van Beest, Kramer, and van Santen.[45] The interatomic distances, correlation functions and angular distributions reported for the starting material[13] are close to those found in our simulation. Samples recovered after compression to 15–20 GPa gave Si-O coordination numbers in the 4.2–4.4 range and angle distributions similar to ours, although more structured. Radial correlations for densified glass have not been reported in Ref. 13.

The MD results indicate that the increased atomic coordination is the main driving force behind most of the transformations encountered by the simulated glass. For the samples recovered after compression, ''irreversible'' densification begins around compressions >6 GPa, the point where Si atoms with O coordination greater than four also appear (Sec. IV D). After this, the amount of densification increases monotonically with the average coordination number up to compressions ≈ 15 GPa, where both coordination and density seem to saturate. These results are in reasonable agreement with the experiments.[5,7,10,52]

The appearance of Si atoms with coordination >4 is also directly connected to the changes found in the computed bond lengths and angles. The changes in the angular distribution functions are in fact directly related to the increased number of Si atoms with octahedral coordination (Sec. IV C). The rather surprising lengthening of the average Si-O bond distance takes place when the bonds are stretched to make room for additional O neighbors. Finally, the broadening of the distance and angle distributions (Table I, Fig. 4), is also clearly linked to the increased population of Si and O atoms with high coordination.

Similar transformations in the average coordination, bond lengths and bond angles are well documented for the x-ray experiments under pressure,[5] while most measurements on densified glass at room conditions detect only a negligible increase in coordination.[3,4] In our opinion, this discrepancy might be partly due to the analysis methods. In the simulation we have found that most of the Si atoms with coordination >4 have Si-O bond distances in the large r tail of the first peak of the $T(r)$. In fact, as shown by Fig. 3 for the densified glass, this peak is asymmetric and definitely not Gaussian. We have estimated the average coordination number by fitting a Gaussian to the simulated $T(r)$, as is often done in the experimental analysis, and erroneously found a small *decrease* of the coordination. The large r tail of the $T(r)$, and thus most of the contribution from the Si atoms with high coordination, is therefore missed by fitting to a single Gaussian. We have found that a direct integration of the simulated $rT(r)$ yields a number of neighbors in agreement with the correct one obtained by a direct analysis of the interatomic distances (as described in Sec. IV C). With this method we reproduce the known coordination increase.

The structural changes in the simulated glass, although less dramatic, resemble the behavior observed in crystalline silica[18,19,57] when the tetrahedral arrangement is replaced by the octahedral coordination as the low-density polymorphs transform into stishovite. The concept of a coordination driven transformation is also consistent with the MD results of Tse, Klug, and Le Page,[13] with the current understanding of the densification process in compressed GeO_2 glass,[25] with a large part of the experimental analysis on silica[3–5,57] and with the model of pressure-induced coordination changes by Stolper and Ahrens[23] and Jeanloz.[24] We are convinced that the high-pressure instability of the tetrahedral network with respect to an increase in coordination, which triggers the irreversible transition from quartz to stishovite, is also the cause of the densification of compressed a-SiO_2. Further experimental and theoretical work is required to verify the validity of these concepts.

ACKNOWLEDGMENTS

This work was supported by the Italian MURST and CNR.

[1] P. W. Bridgman and I. Simon, J. Appl. Phys. **24**, 405 (1953).
[2] J. D. Mackenzie, J. Am. Ceram. Soc. **46**, 461 (1963).
[3] S. Susman, K. J. Volin, R. C. Liebermann, G. D. Gwanmesia, and Y. Wang, Phys. Chem. Glasses **31**, 144 (1990).
[4] S. Susman, K. J. Volin, D. L. Price, M. Grimsditch, and J. P. Rino, R. K. Kalia, P. Vashishta, G. Gwanmesia, Y. Wang, and R. C. Liebermann, Phys. Rev. B **43**, 1194 (1991).
[5] C. Meade, R. J. Hemley, and H. K. Mao, Phys. Rev. Lett. **69**, 1387 (1992).
[6] G. E. Walrafen and P. N. Krishnan, J. Chem. Phys. **74**, 5328 (1981).
[7] M. Grimsditch, Phys. Rev. Lett. **52**, 2379 (1984).
[8] A. Polian and M. Grimsditch, Phys. Rev. B **41**, 6086 (1990).
[9] P. McMillan, B. Piriou, and R. Couti, J. Chem. Phys. **81**, 4235 (1984).
[10] C. S. Zha, R. J. Hemley, H. K. Mao, T. S. Duffy, and C. Meade, Phys. Rev. B **50**, 13 105 (1994).
[11] R. J. Hemley, H. K. Mao, P. M. Bell, and B. O. Mysen, Phys. Rev. Lett. **57**, 747 (1986).
[12] R. A. Murray and W. Y. Ching, Phys. Rev. B **39**, 1320 (1989).
[13] J. S. Tse, D. D. Klug, and Y. Le Page, Phys. Rev. B **46**, 5933 (1992).
[14] W. Jin, R. K. Kalia, P. Vashishta, and J. P. Rino, Phys. Rev. Lett. **71**, 3146 (1993).
[15] L. Stixrude and M. S. T. Bukowinski, Phys. Rev. B **44**, 2523 (1991).
[16] M. S. Somayazulu, S. M. Sharma, N. Garg, S. L. Chaplot, and S. K. Sikka, J. Phys. Condens. Matter **5**, 6345 (1993).
[17] M. S. Somayazulu, S. M. Sharma, and S. K. Sikka, Phys. Rev. Lett. **73**, 98 (1994).
[18] S. Tsuneyuki, M. Tsukada, H. Aoki, and Y. Matsui, Phys. Rev. Lett. **61**, 869 (1988).
[19] L. Liu and W. A. Bassett, *Elements, Oxides and Silicates: High Pressure Phases with Implications for the Earth's Interiors* (New York University Press, New York, 1986).
[20] A. C. Wright, J. Non-Cryst. Solids **179**, 84 (1994).
[21] A. C. Wright, A. G. Clare, D. I. Grimley, and R. N. Sinclair, J. Non-Cryst. Solids **112**, 33 (1989).
[22] S. M. Stishov and S. V. Popova, Geokhimiya **10**, 837 (1961) [Geochemistry **10**, 923 (1961)].
[23] E. M. Stolper and T. J. Ahrens, Geophys. Res. Lett. **14**, 1231 (1987).
[24] R. Jeanloz, Nature (London) **332**, 207 (1988).
[25] K. H. Smith, E. Shero, A. Chizmeshya, and G. H. Wolf, J. Chem. Phys. **102**, 6851 (1995).
[26] M. P. Allen and D. J. Tildesley, *Computer Simulation of Liquids* (Clarendon, Oxford, 1987).
[27] P. Vashishta, R. K. Kalia, J. P. Rino, and I. Ebbsjö, Phys. Rev. B **41**, 12 197 (1990).
[28] B. P. Feuston and S. H. Garofalini, J. Chem. Phys. **89**, 5818 (1988).
[29] B. Vessal, M. Amini, and C. R. A. Catlow, J. Non-Cryst. Solids **159**, 184 (1993).
[30] L. V. Woodcock, C. A. Angell, and P. Cheeseman, J. Chem. Phys. **65**, 1565 (1976).
[31] C. A. Angell, P. A. Cheeseman, and C. C. Phifer, in *Computer-Based Microscopic Description of the Structure and Properties of Materials*, edited by J. Broughton, W. Krakow, and S. T. Pantelides, MRS Symposia Proceedings No. 63 (Materials Research Society, Pittsburgh, 1985), p. 85.
[32] T. F. Soules, J. Chem. Phys. **71**, 4570 (1979); **73**, 4032 (1980).
[33] S. H. Garofalini, J. Chem. Phys. **76**, 3189 (1982).
[34] N. V. Doan, Philos. Mag. A **49**, 683 (1984).
[35] S. K. Mitra, M. Amini, D. Fincham, and R. W. Hockney, Philos. Mag. **43**, 365 (1981).
[36] S. K. Mitra and J. M. Parker, Phys. Chem. Glasses **25**, 95 (1984).
[37] R. L. Erikson and C. J. Hostetler, Geochim. Cosmochim. Acta **51**, 1209 (1987).
[38] J. D. Kubicki and A. C. Lasaga, Am. Mineral. **73**, 941 (1988).
[39] S. Tsuneyuki, Y. Matsui, H. Aoki, and M. Tsukada, Nature (London) **339**, 209 (1989).
[40] S. Tsuneyuki, H. Aoki, and M. Tsukada, Phys. Rev. Lett. **64**, 776 (1990).
[41] R. G. Della Valle and H. C. Andersen, J. Chem. Phys. **94**, 5056 (1991).
[42] R. G. Della Valle and H. C. Andersen, J. Chem. Phys. **97**, 2682 (1992).
[43] R. G. Della Valle and E. Venuti, Chem. Phys. **179**, 411 (1994).
[44] J. R. Rustad, D. A. Yuen, and F. J. Spera, Phys. Rev. A **42**, 2081 (1990).
[45] B. W. H. van Beest, G. J. Kramer, and R. A. van Santen, Phys. Rev. Lett. **64**, 1955 (1990).
[46] W. H. Zachariasen, J. Am. Chem. Soc. **54**, 3841 (1932).
[47] H. C. Andersen, J. Chem. Phys. **72**, 2384 (1980).
[48] W. C. Swope, H. C. Andersen, P. H. Berens, and K. R. Wilson, J. Phys. Chem. **76**, 637 (1982).
[49] J. F. Fox and H. C. Andersen, J. Phys. Chem. **88**, 4019 (1984).
[50] D. Brown and J. H. R. Clarke, Mol. Phys. **51**, 1243 (1984).
[51] R. L. Mozzi and B. E. Warren, J. Appl. Crystallogr. **2**, 164 (1969).
[52] A. Polian and M. Grimsditch, Phys. Rev. B **47**, 13 979 (1993).
[53] D. I. Grimley, A. C. Wright, and R. N. Sinclair, J. Non-Cryst. Solids **119**, 49 (1990).
[54] R. A. B. Devine, R. Dupree, I. Farnan, and J. J. Capponi, Phys. Rev. B **35**, 2560 (1987).
[55] R. A. B. Devine and J. Arndt, Phys. Rev. B **35**, 9376 (1987).
[56] P. G. Coombs, J. F. De Natale, P. J. Hood, D. K. McElfresh, R. S. Wortman, and J. F. Shackelford, Philos. Mag. B **51**, L39 (1985).
[57] R. J. Hemley, in *High-Pressure Research in Mineral Physics*, edited by M. H. Manghanni and Y. Syono (Terra Scientific, Tokyo, 1987), p. 347.
[58] J. H. Konnert and J. Karle, Acta Crystallogr. **A29**, 702 (1973).